





Vacancy-engineered flat-band superconductivity in holey graphene

Matheus S. M. de Sousa ¹, Fujun Liu ², Fanyao Qu ², and Wei Chen ¹

¹*Department of Physics, PUC-Rio, 22451-900 Rio de Janeiro, Brazil*

²*Instituto de Física, Universidade de Brasília, Brasília-DF 70919-970, Brazil*



(Received 19 October 2021; accepted 12 January 2022; published 19 January 2022)

A bipartite lattice with chiral symmetry is known to host zero-energy flat bands if the numbers of the two sublattices are different. We demonstrate that this mechanism of producing flat bands can be realized on graphene by introducing periodic vacancies. Using first-principles calculations, we elaborate that even though pristine graphene does not exactly preserve chiral symmetry, this mechanism applied to holey graphene still produces single or multiple bands as narrow as ~ 0.5 eV near the Fermi surface throughout the entire Brillouin zone. Moreover, this mechanism can combine with vacancy-engineered nonsymmorphic symmetry to produce band structures with coexisting flat bands and nodal lines. A weak coupling mean-field treatment suggests the stabilization of superconductivity by these vacancy-engineered narrow bands. In addition, superconductivity occurs predominantly on the majority sublattices, with an amplitude that increases with the number of narrow bands.

DOI: [10.1103/PhysRevB.105.014511](https://doi.org/10.1103/PhysRevB.105.014511)

I. INTRODUCTION

The superconductivity (SC) discovered recently in twisted bilayer graphene (TBLG) revives interest in the search for SC on graphene-based materials [1]. While the origin of the observed SC is still under intense debate, the small flat band due to splitting and anticrossing of the Dirac cones from the two graphene sheets is generally considered to play an important role [2–8]. In fact, the possibility of flat band induced SC has long been of great interest, since the CuO_2 plane of high-temperature superconductor materials [9–11], at which the SC occurs [12–14], has the same structure (if Cu and O are not distinguished) as the Lieb lattice that is known to host a flat band and has been realized in various other systems [15–25]. On the other hand, from the density of states (DOS) point of view, it is intriguing to ask whether there exists some generic mechanisms that can generate flat bands in a large area of the Brillouin zone (BZ) of single-layer graphene at low energy, such that SC may be stabilized.

In this paper, we elaborate that the generic mechanism of producing zero-energy flat bands (ZEFBs) on any bipartite lattice, put forward by Sutherland [26] and Lieb [27], can be realized on graphene by introducing periodic vacancies. Lieb's theorem states that on a bipartite lattice with chiral (sublattice) symmetry, ZEFBs occur if the numbers of the two sublattices per unit cell are different, $N_A \neq N_B$, and the ZEFBs are at least $|N_A - N_B|$ -fold degenerate. We demonstrate that this situation can be created on the honeycomb lattice by removing different numbers of the two sublattices in an enlarged unit cell, and ZEFBs throughout the entire BZ occur, provided the tight-binding model of the lattice preserves the chiral symmetry. This mechanism is then tested in realistic single-layer graphene by first-principles calculations. Our results indicate that despite graphene in reality not exactly preserving chiral symmetry, this mechanism can still produce bands as narrow

as ~ 0.5 eV near the Fermi surface throughout the entire BZ, and moreover can be used to engineer an exotic band structure that contains both flat bands and nodal lines.

Our theoretical investigation is largely motivated by the fact that graphene with vacancies, often called holey graphene or graphene nanomesh, has been realized by various experimental techniques, such as nitrogenation [28,29], self-aligned anisotropic etching [30], nanonetwork masking [31], and lithography using copolymer [32], nanosphere [33], or He ion beams [34], suggesting the feasibility of vacancy engineering in reality. Note that our proposal considers complete removal of carbon atoms, which is in contrast to the flat bands produced by the periodic potentials from adatoms [35], requires much less removal of atoms compared to the cyclicgraphyne [36] or azite [37] proposals, and may also be realizable in superlattices nanolithographed in semiconductor thin films [38].

In addition, since these vacancy-engineered narrow bands dramatically enlarge the DOS at the Fermi surface compared to pristine graphene, we examine the possibility of phonon-mediated SC by means of a weak coupling mean-field theory using the realistic phonon bandwidth [39–42]. Note that this type of mean-field theory is usually disregarded for pristine graphene since the vanishing DOS at the Dirac point does not support phonon-mediated pairing. In addition, the SC discovered in TBLG likely originated from strong electron-electron correlations [1]. However, we elaborate that, owing to the enlarged DOS, the conventional phonon-mediated weak-coupling SC can be stabilized by these vacancy-engineered flat bands without any additional electron-electron correlations. The spatial pattern of pairing is highly influenced by the chiral symmetric wave function of the ZEFBs, with a magnitude that increases with the number of ZEFBs, pointing to the possibility of enhancing critical temperature via increasing the number of flat bands.

The structure of the paper is organized in the following manner. In Sec. II, we first revisit Lieb's theorem with an emphasis on the chiral symmetry of the ZEFB wave functions. Two vacancy configurations are then used to demonstrate perfect ZEFBs on a honeycomb lattice that preserves chiral symmetry. The narrow bands of these two configurations realized in graphene are then elaborated by first-principle calculations, and additionally another vacancy configuration that yields coexisting narrow bands and nodal lines. In Sec. III, we lay out the weak-coupling mean-field theory to investigate SC on the first two vacancy configurations, especially to detail their spatial pattern and dependence on the pairing interaction and degeneracy of the ZEFBs. These results are summarized in Sec. IV.

II. VACANCY-ENGINEERED FLAT BANDS ON GRAPHENE

A. Chiral symmetry and rank-nullity theorem

We first revisit Lieb's theorem that is based on the rank-nullity theorem [27], with a special emphasis on the nonspatial symmetries, localization of the wave functions, and applications to periodic vacancies. We consider any two- (2D) or three-dimensional (3D) bipartite-lattices described by single-particle Hamiltonian $H(\mathbf{k})$ in momentum space that preserves time-reversal, particle-hole (PH) chiral symmetries,

$$\begin{aligned} TH(\mathbf{k})T^{-1} &= H(-\mathbf{k}), \\ CH(\mathbf{k})C^{-1} &= -H(-\mathbf{k}), \\ SH(\mathbf{k})S^{-1} &= -H(\mathbf{k}), \end{aligned} \quad (1)$$

which are nonspatial symmetries particularly relevant to topological order [43–46] and topological phase transitions [47]. In these bipartite lattices, the Hamiltonian matrix arranged in the basis of the electron operators of the two sublattices ($c_{B\mathbf{k}}, c_{A\mathbf{k}}$) is a block-off-diagonal 2×2 matrix, and the symmetry operators are implemented by $T = K$, $C = \sigma_3 K$, and $S = \sigma_3$, where K is the complex conjugation operator.

Now suppose we enlarge the unit cell to contain not two but $N = \text{even}$ number of sites with the same amount of two sublattices. Before any vacancy has been introduced into the lattice, the Hamiltonian matrix arranged in the basis ($c_{B_1\mathbf{k}}, \dots, c_{B_{N/2}\mathbf{k}}, c_{A_1\mathbf{k}}, \dots, c_{A_{N/2}\mathbf{k}}$) remains block-off-diagonal

$$H(\mathbf{k}) = \begin{pmatrix} & Q(\mathbf{k}) \\ Q^\dagger(\mathbf{k}) & \end{pmatrix}, \quad (2)$$

where $Q(\mathbf{k})$ is an $(N/2) \times (N/2)$ square matrix. The symmetry operators are implemented by $C = \sigma_3 \otimes I_{N/2} K$ and $S = \sigma_3 \otimes I_{N/2}$ in this case, with $I_{N/2}$ the $(N/2) \times (N/2)$ identity matrix. If we now introduce periodic vacancies into the lattice, the columns and rows in the $H(\mathbf{k})$ in Eq. (2) that correspond to the vacancy sites will be removed. It is then obvious that if the number of vacancies on the A and B sublattices are different, then the unit cell will contain a different number of sublattices $N_A \neq N_B$. As a result, the $Q(\mathbf{k})$ in Eq. (2) as an $N_A \times N_B$ matrix is not a square matrix anymore, as elaborated in Fig. 1. Nevertheless, the PH and chiral symmetries of the systems still hold since removing the columns and rows in $C = \sigma_3 \otimes I_{N/2} K$ and $S = \sigma_3 \otimes I_{N/2}$ that correspond to the vacancy sites preserve Eqs. (1). As a result, the band structure at any vacancy configuration is PH symmetric, and the ZEFB

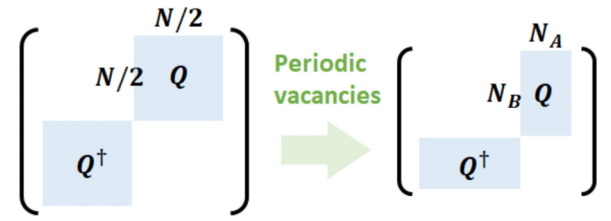


FIG. 1. Schematics of the proposed generic mechanism for ZEFBs. Starting from a chiral symmetric bipartite lattice, the Hamiltonian matrix $H(\mathbf{k})$ describing an enlarged unit cell containing $N_A = N_B = N/2$ sites of each sublattice is block-off-diagonal (blue blocks). After periodic vacancies are introduced, which correspond to removing some columns and rows in the Hamiltonian, the off-diagonal block becomes not square if the unit cell contains different numbers of the two sublattices $N_B > N_A$. In this case, the rank-nullity theorem ensures that ZEFBs must occur.

wave functions must be localized on one of the two sublattices since they are eigenstates of the chiral operator S . In fact, we will prove below that the ZEFB wave functions must localize in the majority sublattices.

Denoting $r(M)$ as the rank and $\eta(M)$ as the nullity of a matrix M , our interest is in how the nullity of the Hamiltonian $\eta(H)$, which counts the number of ZEFBs, can be nonzero. Without loss of generality, we assume that the vacancy configuration is such that the B sublattices are the majority $N_B > N_A$, causing Q not to be square. In this case, the rank-nullity theorem states that

$$r(Q) + \eta(Q) = N_A, \quad r(H) + \eta(H) = N_A + N_B. \quad (3)$$

For H of the form of Eq. (2) with a Q that is not square, the rank satisfies

$$\begin{aligned} r(Q) &= r(Q^\dagger) = r(QQ^\dagger) = r(Q^\dagger Q), \\ r(H) &= r(Q) + r(Q^\dagger) = 2r(Q). \end{aligned} \quad (4)$$

Using these simple identities in linear algebra, we now prove the following propositions.

Proposition 1: $\eta(H) > 0$ if Q is not square. This can be proved easily from Eqs. (3) and (4):

$$\eta(H) = N_A + N_B - 2r(Q) = N_B - N_A + 2\eta(Q). \quad (5)$$

Hence $\eta(H) > 0$ if $N_B > N_A$, meaning that ZEFB must emerge if we remove the two sublattices in different quantities.

Proposition 2: $\eta(H) = N_B - N_A$ if $\eta(Q) = 0$. To prove this, we start from

$$r(QQ^\dagger) + \eta(QQ^\dagger) = N_B, \quad r(Q^\dagger Q) + \eta(Q^\dagger Q) = N_A, \quad (6)$$

which implies

$$r(QQ^\dagger) - r(Q^\dagger Q) = N_B - N_A. \quad (7)$$

If Q itself is not singular, $\eta(Q) = 0$, which is true in many practical examples, then Eqs. (3) implies $r(Q) = N_A = r(QQ^\dagger) = r(Q^\dagger Q)$. Then, from Eqs. (6), one sees that $\eta(QQ^\dagger) = N_B - N_A$ and $\eta(Q^\dagger Q) = 0$. Because the square of the Hamiltonian $H^2 = \text{diag}(QQ^\dagger, Q^\dagger Q)$ has the same nullity and ZEFB wave functions as H , we immediately see that

$\eta(H) = \eta(H^2) = \eta(QQ^\dagger) = N_B - N_A$. Propositions 1 and 2 constitute the original version of Lieb's theorem [26,27,48].

Proposition 3: ZEFB wave functions are localized in the majority sublattices if $\eta(Q) = 0$. This is simply because the proof for proposition 2 shows that the ZEFB wave functions are given by diagonalizing the first block QQ^\dagger in H^2 that belongs to the majority B sublattices, whereas wave functions in A sublattices are zero.

We aim to examine these propositions in the spinless honeycomb lattice with nearest-neighbor hopping

$$H = \sum_{\langle ij \rangle} t c_i^\dagger c_j + U \sum_{i \in v} c_i^\dagger c_i, \quad (8)$$

owing its relevance to the p_z orbital of single-layer graphene that will be addressed later, where c_i denotes the electron annihilation operator at site i , and U is the large on-site potential that can be used to conveniently project out the vacancy sites $i \in v$. Increasing from $U = 0$ to $U > 100t$ can continuously change the band structure from Dirac points to ZEFBs, similar to that proposed recently in the Lieb-kagome lattices [49], but we will focus on the large on-site potential regime $U > 100t$ that completely removes the vacancy sites. We denote these vacancy configurations by $C_{N_A+N_B}$. In the left panel of Fig. 2(a), we show a C_{15} example of removing a single A sublattice from a $N = 16$ rectangular unit cell such that $N_A = 7$ and $N_B = 8$. In this case, the BZ is rectangular and the PH symmetric tight-binding band structure plotted along a high-symmetry line clearly indicates a single ZEFB throughout the BZ, as shown in the left panel of Fig. 2(b). In contrast, the C_{14} configuration shown in the right panel of Figs. 2(a) and 2(b) that removes two A sublattices on the same 16-site unit cell, such that $N_A = 6$ and $N_B = 8$, has doubly degenerate ZEFBs $\eta(H) = N_B - N_A = 2$, consistent with proposition 2. In Appendix, we also elaborate on proposition 3 by presenting the wave functions of the ZEFBs for C_{15} and C_{14} and show that indeed both are localized on the majority B sublattices. Finally, we remark that although we focus on periodic vacancies on an infinite graphene, propositions 1–3 also explain the number of zero eigenenergies and their wave functions of finite-size graphene with random vacancies [50].

B. Application to realistic graphene

To examine the proposed mechanism on realistic single-layer graphene, it should be first noted that graphene, in reality, does not exactly preserve the PH and chiral symmetries in Eqs. (1) owing to the complications such as longer range hopping and hybridization between different orbitals, although magnitudes of these factors are much smaller than the nearest-neighbor hopping [51]. To investigate the effect of these symmetry-breaking factors, we turn to density functional theory (DFT) to obtain the band structure of graphene with periodic vacancies. In Fig. 2(c), we show the DFT band structures and DOS for C_{15} and C_{14} , which indicate that very narrow bands do occur near the Fermi surface. Although not perfectly flat, these bands are as narrow as ~ 0.5 eV, reminisce the ZEFBs. Moreover, the DOS at the Fermi surface is dramatically enhanced by these narrow bands compared to pristine graphene, as indicated by Fig. 2(d).

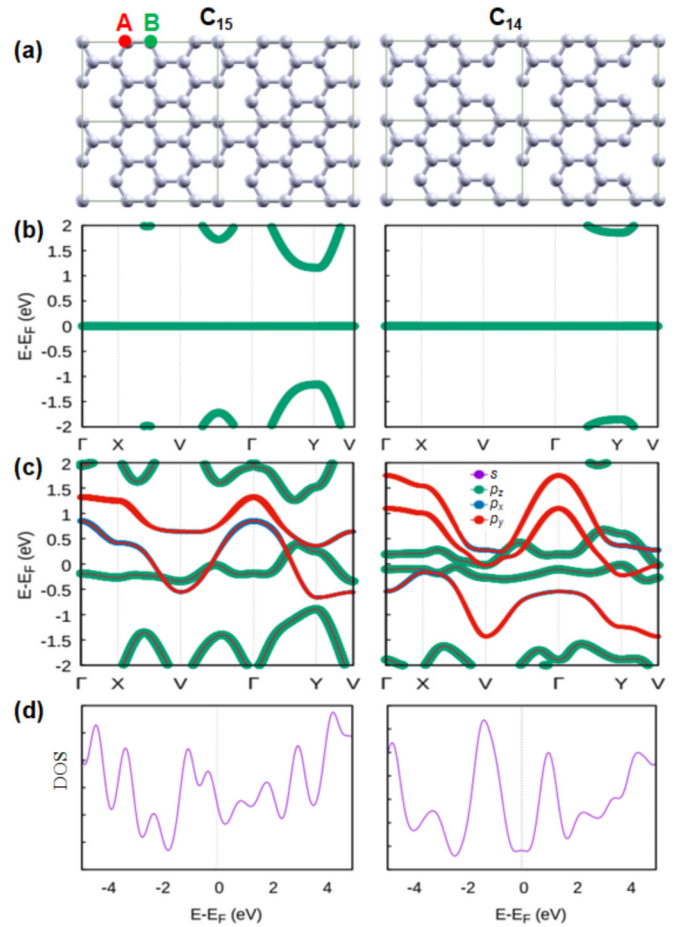


FIG. 2. Numerical results for the two vacancy configurations C_{15} (left column) and C_{14} (right column), whose lattice structures are shown in (a) with the two sublattices A and B indicated. (b) The band structures obtained from the nearest-neighbor tight-binding model that preserves chiral symmetry, which contains a single ZEFB for C_{15} and doubly degenerate ZEFBs for C_{14} . (c) DFT band structures and (d) the corresponding DOS for these two vacancy configurations realized by graphene that does not exactly preserve the chiral symmetry, which still yield very narrow bands of mainly p_z at low energy.

C. Coexistence of ZEFBs and nodal lines

We proceed to demonstrate that the proposed mechanism can coexist with another vacancy engineering principle proposed recently, namely, the nodal-line semimetals caused by 2D nonsymmorphic vacancy configurations [52–54]. In these nonsymmorphic configurations, every two carbon atoms map to each other under glide plane operation, resulting in nodal lines at the BZ boundary regardless of the details of the Hamiltonian [55–58]. Although these nodal lines are based on point group symmetry while the flat bands are based on the rank-nullity theorem, which are two completely distinct mechanisms, they may manifest simultaneously in some vacancy configurations. As an example, in Fig. 3 we show a C_{22} configuration that contains two vacancies on the A sublattice, and additionally a glide plane along the \hat{x} direction. The resulting DFT band structure indicates that both mechanisms prevail in this situation, yielding a band structure that contains two low-energy narrow bands that reminisce doubly

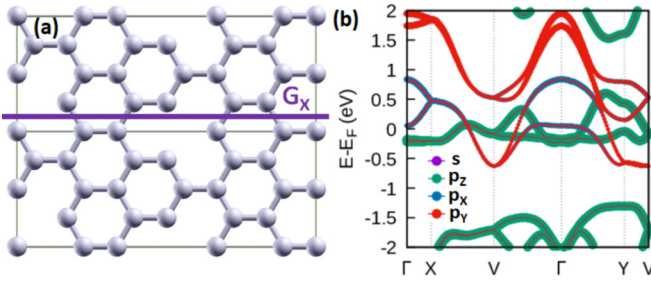


FIG. 3. (a) A vacancy configuration C_{22} that contains two missing A sublattices and a glide plane G_x . (b) The resulting band structure contains two low-energy narrow bands of mainly p_z orbital origin and, in addition, every two pairs of spin degenerate bands stick together to form fourfold degenerate nodal lines at the $X - V$ section of the BZ boundary.

degenerate ZEFBs, and in addition every two pairs of bands (each pair is spin degenerate) stick together at the BZ boundary $k_x = 0$ [the $X - V$ section of Fig. 3(b)] to form symmetry-enforced nodal lines as predicted. This example indicates that vacancy engineering can combine different crystalline and nonspatial symmetries to produce very exotic band structures that may not be easily found in nature.

III. MEAN-FIELD TREATMENT OF SC STABILIZED BY ZEFBs

A. Bogoliubov-de Gennes equations for graphene with periodic vacancy

The enlarged DOS near the Fermi surface due to the narrow bands is expected to dramatically change the electronic and magnetic properties of holey graphene compared to pristine graphene. However, these narrow bands are neither perfectly flat nor entirely located at zero energy, and hence it is unclear at present whether strong correlations will play an important role on the electronic properties in the same way as in TBLG [1]. On the other hand, the phonon bandwidth in graphene is about $\omega_D \approx 0.25$ eV [39–42], which means that the narrow bands with bandwidth ~ 0.5 eV in a large area of the BZ are within the Debye frequency, suggesting a large phase space for phonon-mediated Cooper pairing [59,60]. These features motivate us to examine whether a conventional phonon-mediated s -wave SC phase emerges in holey graphene with low-energy narrow bands. For this purpose, we resort to the following spinful mean-field model of s -wave SC,

$$H = \sum_{\langle ij \rangle \sigma} t c_{i\sigma}^\dagger c_{j\sigma} + \sum_{\langle\langle ij \rangle\rangle \sigma} t' c_{i\sigma}^\dagger c_{j\sigma} - \sum_{i\sigma} \mu c_{i\sigma}^\dagger c_{i\sigma} + \sum_i (\Delta_i c_{i\uparrow}^\dagger c_{i\downarrow}^\dagger + \Delta_i^* c_{i\downarrow} c_{i\uparrow}) + U \sum_{i \in v} c_{i\sigma}^\dagger c_{i\sigma}, \quad (9)$$

where $t = 2.8$ eV is the nearest-neighbor hopping on the honeycomb lattice, Δ_i is the local pairing amplitude at site i , and the on-site potential $U > 100t$ is used to project out the vacancy sites $i \in v$. We use the next-nearest-neighbor hopping t' and chemical potential μ to simulate the breaking of chiral symmetry in realistic graphene, and find that the values $t' = -0.2$ eV and $\mu = 0.2$ eV can give a reasonable fit to

the narrow bands obtained by DFT in both C_{15} and C_{14} , as demonstrated in the Appendix.

The mean-field Hamiltonian is diagonalized into $H = \text{const} + \sum_{\mathbf{k}\alpha} E_{\mathbf{k}} \gamma_{\mathbf{k}\alpha}^\dagger \gamma_{\mathbf{k}\alpha}$ by a Bogoliubov transformation

$$c_{i\uparrow} = \sum_{\mathbf{k}} \gamma_{\mathbf{k}\uparrow} u_{\mathbf{k}}(i) - \gamma_{\mathbf{k}\downarrow}^\dagger v_{\mathbf{k}}^*(i), \\ c_{i\downarrow} = \sum_{\mathbf{k}} \gamma_{\mathbf{k}\downarrow} u_{\mathbf{k}}(i) + \gamma_{\mathbf{k}\uparrow}^\dagger v_{\mathbf{k}}^*(i), \quad (10)$$

where $i = 1, 2, \dots, N_A + N_B$ denotes the site inside a unit cell, and $\gamma_{\mathbf{k}\sigma}$ is the annihilation operator of the Bogoliubov quasiparticles. The wave functions $\{u_{\mathbf{k}}(i), v_{\mathbf{k}}(i)\}$ and eigenenergy $E_{\mathbf{k}}$ satisfy

$$E_{\mathbf{k}} u_{\mathbf{k}}(i) = \sum_{\langle ij \rangle} t u_{\mathbf{k}}(j) + \sum_{\langle\langle ij \rangle\rangle} t' u_{\mathbf{k}}(j) + U \delta_{i \in v} u_{\mathbf{k}}(i) + \Delta_i v_{\mathbf{k}}(i), \\ E_{\mathbf{k}} v_{\mathbf{k}}(i) = - \sum_{\langle ij \rangle} t v_{\mathbf{k}}(j) - \sum_{\langle\langle ij \rangle\rangle} t' v_{\mathbf{k}}(j) - U \delta_{i \in v} v_{\mathbf{k}}(i) + \Delta_i^* u_{\mathbf{k}}(i). \quad (11)$$

Having found the wave functions and eigenenergies of the quasiparticles, we determine the pairing amplitude at site i by

$$\Delta_i = \sum_{\mathbf{k}} V \theta(\omega_D - E_{\mathbf{k}}) [2f(E_{\mathbf{k}}) - 1] u_{\mathbf{k}}(i) v_{\mathbf{k}}^*(i), \quad (12)$$

where $f(E_{\mathbf{k}}) = (e^{E_{\mathbf{k}}/k_B T} + 1)^{-1}$ is the Fermi distribution and $V < 0$ is the pairing interaction acting within Debye frequency $\omega_D = 0.25$ eV, as ensured by the step function $\theta(\omega_D - E_{\mathbf{k}})$. Equations (11) and (12) are solved self-consistently until the local pairing amplitude Δ_i converges at a given pairing interaction and temperature $\{V, T\}$. We will consider only s -wave pairing since the chiral symmetry of the flat-band wave function limits the pairing to be between the same sublattices, favoring on-site pairing while ruling out nearest-neighbor pairing. Longer range pairing may, in principle, be possible by correctly incorporating phonons at finite momentum, which should be addressed elsewhere.

B. Numerical results for the local pairing

Numerical calculation of our mean-field theory applied to pristine graphene yields $\Delta_i = 0$ everywhere, consistent with the experimental observation that single-layer pristine graphene has no SC. It is perhaps for this reason that such a simple mean-field theory has not been considered relevant to any pairing mechanism in graphene. However, our numerical results indicate that a conventional phonon-mediated pairing can be stabilized by the vacancy-engineered flat bands and are well-described by such a simple mean-field theory. In Figs. 4(a) and 4(b), we show the local gap Δ_i at zero temperature for the two vacancy configurations C_{15} and C_{14} illustrated in Fig. 2. Our result indicates a finite Δ_i in holey graphene and, moreover, Δ_i on the B sublattices is about two orders of magnitude larger than that on the A sublattices. This feature stems from the fact that the chiral symmetry breaking terms are relatively small $\{t', \mu\} \ll t$, so the narrow band wave functions still roughly satisfy proposition 3 in

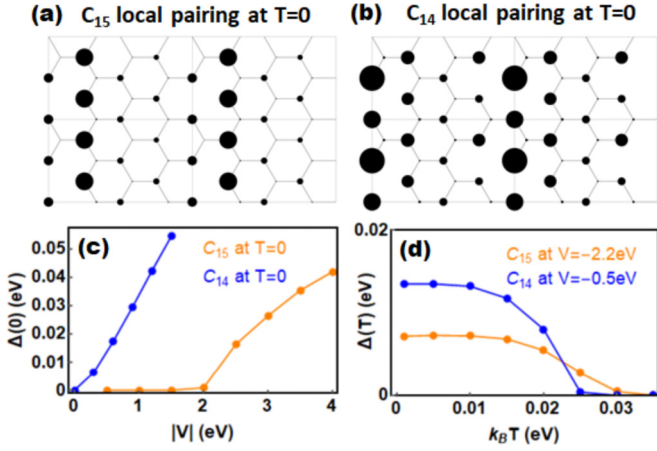


FIG. 4. (a) Local pairing amplitude Δ_i represented by circle size for the C_{15} configuration in Fig. 2, calculated at zero temperature and pairing interaction $V = -2.2$ eV by our weak coupling mean-field model. The largest circles correspond to $\Delta_i = 0.036$ eV. (b) Δ_i for the C_{14} configuration in Fig. 2 at zero temperature and pairing interaction $V = -0.5$ eV, where the largest circles correspond to $\Delta_i = 0.074$ eV. In these two figures, one sees that the B sublattices that the vacancy sites do not belong to have much larger pairing amplitude. (c) Spatially averaged pairing amplitude at zero temperature $\Delta(0)$ versus the pairing interaction $|V|$. (d) The spatially average pairing amplitude $\Delta(T)$ as a function of temperature.

Sec. II A and hence are mainly localized on the B sublattices, as discussed in Appendix. For C_{15} , the spatially averaged gap $\Delta(T) = \sum_i \Delta_i / (N_A + N_B)$ at zero temperature $\Delta(0)$ is vanishingly small at small pairing potential V . Only when the pairing potential has the same order of magnitude as the hopping $|V| \sim t$ does a sizable gap emerge, implying that a sufficiently strong electron-phonon interaction is needed to support SC in C_{15} . On the other hand, C_{14} requires much smaller $|V|$ to trigger SC in comparison with C_{15} , suggesting that increasing the number of narrow bands does help to create the SC phase. Concerning the temperature dependence, the spatially averaged gap shows a trend similar to the usual weak coupling superconductors, which vanishes at a critical temperature T_c that is higher at larger pairing potential V . In addition, T_c is generally raised in the configurations with more narrow bands, consistent with that expected from an enlarged DOS. Since the proposed engineering mechanism in principle has no restriction on the number of narrow bands $N_B - N_A$ (times 2 if including spin), we anticipate that the vacancy configurations with very different numbers of the two sublattices may yield a very high T_c , which is presumably more likely to engineer in configurations with a larger unit cell.

IV. CONCLUSIONS

In summary, we demonstrate that Lieb's theorem of ZEFBs can be realized on graphene by introducing periodic vacancies, which can be experimentally relevant to holey graphene or graphene nanomesh. Although graphene in reality does not preserve the chiral symmetry required by the theorem, periodic vacancies can still induce bands as narrow as ~ 0.5 eV near the Fermi surface because the symmetry breaking factors

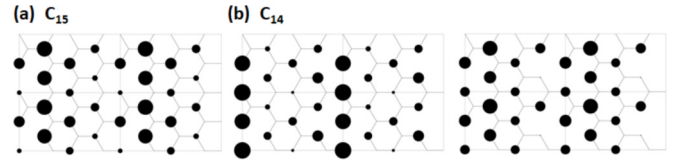


FIG. 5. Wave functions $|\psi_i|^2$ at momentum $\mathbf{k} = (0.15, 0.37)$ of (a) the single ZEFB of C_{15} and (b) the two degenerate ZEFBs of C_{14} with only nearest-neighbor hopping, whose band structure is that shown in Fig. 2(b). The largest circles correspond to $|\psi_i|^2 = 0.313$. All these wave functions preserve chiral symmetry and hence are localized only on the majority B sublattices.

are relatively weak compared to the nearest-neighbor hopping. Moreover, our results suggest that periodic vacancies can be used to combine various nonspatial and crystalline symmetries to produce very exotic band structures, such as the coexisting ZEFBs and nodal lines revealed in the present paper, paving a way to engineer band structures of 2D materials beyond the limitation set by the underlying crystalline structures.

The vacancy-engineered narrow bands dramatically enlarge the DOS near the Fermi surface, and hence are expected to significantly change the electronic and magnetic properties of the holey graphene compared to the pristine one, which await further investigations. In particular, we reveal that a phonon-mediated conventional SC can be stabilized without the need of any other electronic correlations, and can be described by a simple mean-field theory. The local pairing amplitude is highly localized on the majority sublattices, a feature originating from the chiral symmetry of the flat-band wave functions. The minimal electron-phonon interaction required to create the SC phase varies significantly with the number of narrow bands, but increasing the numbers of narrow bands generally reduces the minimal electron-phonon interaction, as expected from the DOS point of view. As a

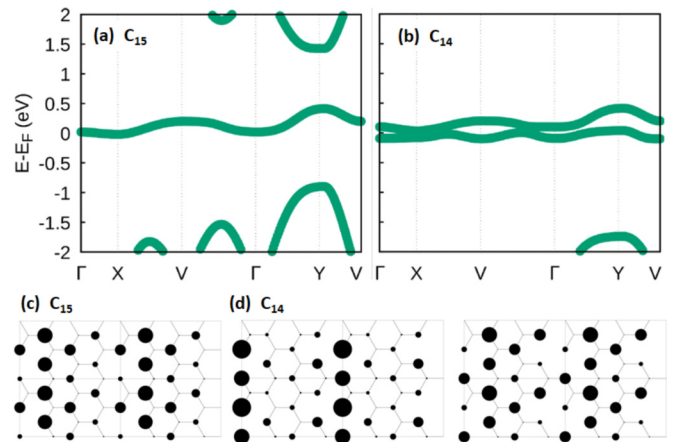


FIG. 6. Tight-binding band structure of (a) C_{15} and (b) C_{14} with $t = 2.8$ eV, $t' = -0.2$ eV, and $\mu = 0.2$ eV, which yields a reasonable fit to the p_z orbital bands obtained from DFT shown in Fig. 2(c). The wave functions $|\psi_i|^2$ of the narrow bands at momentum $\mathbf{k} = (0.15, 0.37)$ are shown in (c) and (d), which are still highly localized on the B sublattices since the chiral symmetry breaking terms are relatively weak, $\{t', \mu\} \ll t$.

result, we anticipate that a certain experimental effort to search for the appropriate vacancy configuration that has a sufficient number of narrow bands is needed to observe the SC.

APPENDIX: FLAT-BAND WAVE FUNCTIONS WITH AND WITHOUT CHIRAL SYMMETRY

Proposition 3 in Sec. II A states that the ZEFB wave functions for a chiral symmetric system in any vacancy configuration must localize on the majority sublattices. As an example, in Fig. 5 we show the single flat-band wave function for C_{15} and the two degenerate flat-band wave functions for C_{15} at momentum $\mathbf{k} = (0.15, 0.37)$, both described by a spinless nearest-neighbor hopping Hamiltonian $H = \sum_{\langle ij \rangle} t c_i^\dagger c_j$ that preserves chiral symmetry. We find that all these wave functions are localized in the majority B sublattices where the vacancies do not belong, satisfying the proposition 3 in Sec. II A.

For the realistic graphene that does not preserve chiral symmetry, we rely on numerical calculations to investigate the wave functions. Using a tight-binding model with nearest t and next-nearest-neighbor hopping t' , and additionally a chemical potential μ [described by the Hamiltonian in Eq. (9) without pairing and spin], we find that the parameters $t = 2.8$ eV, $t' = -0.2$ eV, and $\mu = 0.2$ eV can fit the p_z orbital bands of the DFT band structure shown in Fig. 2(c) reasonably well, as shown in Figs. 6(a) for C_{15} and 6(b) for C_{14} . The wave functions of the narrow bands close to the Fermi surface are shown in Figs. 6(c) and 6(d) at the same momentum $\mathbf{k} = (0.15, 0.37)$ as that shown in Figs. 5(a) and 5(b). We find that because these chiral symmetry breaking terms $\{t', \mu\}$ are relatively small compared to t , the wave functions on the majority B sublattices are about two orders of magnitude larger than that on the minority A sublattices. In other words, the wave function still roughly preserves the chiral symmetry and approximately satisfies proposition 3 in Sec. II A. As a result, the local pairing amplitude in the SC phase is much larger on B sublattices, as shown in Fig. 4.

-
- [1] Y. Cao, V. Fatemi, S. Fang, K. Watanabe, T. Taniguchi, E. Kaxiras, and P. Jarillo-Herrero, *Nature (London)* **556**, 43 (2018).
- [2] E. Suárez Morell, J. D. Correa, P. Vargas, M. Pacheco, and Z. Barticevic, *Phys. Rev. B* **82**, 121407(R) (2010).
- [3] R. Bistritzer and A. H. MacDonald, *Proc. Natl. Acad. Sci. USA* **108**, 12233 (2011).
- [4] P. Moon and M. Koshino, *Phys. Rev. B* **85**, 195458 (2012).
- [5] G. Trambly de Laissardière, D. Mayou, and L. Magaud, *Phys. Rev. B* **86**, 125413 (2012).
- [6] J. M. B. Lopes dos Santos, N. M. R. Peres, and A. H. Castro Neto, *Phys. Rev. B* **86**, 155449 (2012).
- [7] S. Fang and E. Kaxiras, *Phys. Rev. B* **93**, 235153 (2016).
- [8] Y. Cao, V. Fatemi, A. Demir, S. Fang, S. L. Tomarken, J. Y. Luo, J. D. Sanchez-Yamagishi, K. Watanabe, T. Taniguchi, E. Kaxiras, R. C. Ashoori, and P. Jarillo-Herrero, *Nature (London)* **556**, 80 (2018).
- [9] J. G. Bednorz and K. A. Müller, *Z. Phys. B: Condens. Matter* **64**, 189 (1986).
- [10] P. A. Lee, N. Nagaosa, and X.-G. Wen, *Rev. Mod. Phys.* **78**, 17 (2006).
- [11] B. Keimer, S. A. Kivelson, M. R. Norman, S. Uchida, and J. Zaanen, *Nature (London)* **518**, 179 (2015).
- [12] P. W. Anderson, *Science* **235**, 1196 (1987).
- [13] V. J. Emery, *Phys. Rev. Lett.* **58**, 2794 (1987).
- [14] F. C. Zhang and T. M. Rice, *Phys. Rev. B* **37**, 3759 (1988).
- [15] R. Shen, L. B. Shao, B. Wang, and D. Y. Xing, *Phys. Rev. B* **81**, 041410(R) (2010).
- [16] D. Guzmán-Silva, C. Mejía-Cortés, M. A. Bandres, M. C. Rechtsman, S. Weimann, S. Nolte, M. Segev, A. Szameit, and R. A. Vicencio, *New J. Phys.* **16**, 063061 (2014).
- [17] S. Mukherjee, A. Spracklen, D. Choudhury, N. Goldman, P. Öhberg, E. Andersson, and R. R. Thomson, *Phys. Rev. Lett.* **114**, 245504 (2015).
- [18] S. Taie, H. Ozawa, T. Ichinose, T. Nishio, S. Nakajima, and Y. Takahashi, *Sci. Adv.* **1**, e1500854 (2015).
- [19] R. A. Vicencio, C. Cantillano, L. Morales-Inostroza, B. Real, C. Mejía-Cortés, S. Weimann, A. Szameit, and M. I. Molina, *Phys. Rev. Lett.* **114**, 245503 (2015).
- [20] A. Julku, S. Peotta, T. I. Vanhala, D.-H. Kim, and P. Törmä, *Phys. Rev. Lett.* **117**, 045303 (2016).
- [21] S. Xia, Y. Hu, D. Song, Y. Zong, L. Tang, and Z. Chen, *Opt. Lett.* **41**, 1435 (2016).
- [22] F. Diebel, D. Leykam, S. Kroesen, C. Denz, and A. S. Desyatnikov, *Phys. Rev. Lett.* **116**, 183902 (2016).
- [23] M. R. Slot, T. S. Gardenier, P. H. Jacobse, G. C. P. van Miert, S. N. Kempkes, S. J. M. Zevenhuizen, C. M. Smith, D. Vanmaekelbergh, and I. Swart, *Nat. Phys.* **13**, 672 (2017).
- [24] S. Klembt, T. H. Harder, O. A. Egorov, K. Winkler, H. Suchomel, J. Beierlein, M. Emmerling, C. Schneider, and S. Höfling, *Appl. Phys. Lett.* **111**, 231102 (2017).
- [25] B. Cui, X. Zheng, J. Wang, D. Liu, S. Xie, and B. Huang, *Nat. Commun.* **11**, 66 (2020).
- [26] B. Sutherland, *Phys. Rev. B* **34**, 5208 (1986).
- [27] E. H. Lieb, *Phys. Rev. Lett.* **62**, 1201 (1989).
- [28] R. Pawlak, X. Liu, S. Ninova, P. D'Astolfo, C. Drechsel, S. Sangtarash, R. Häner, S. Decurtins, H. Sadeghi, C. J. Lambert, U. Aschauer, S.-X. Liu, and E. Meyer, *J. Am. Chem. Soc.* **142**, 12568 (2020).
- [29] J. Mahmood, E. K. Lee, M. Jung, D. Shin, I.-Y. Jeon, S.-M. Jung, H.-J. Choi, J.-M. Seo, S.-Y. Bae, S.-D. Sohn, N. Park, J. H. Oh, H.-J. Shin, and J.-B. Baek, *Nat. Commun.* **6**, 6486 (2015).
- [30] Z. Shi, R. Yang, L. Zhang, Y. Wang, D. Liu, D. Shi, E. Wang, and G. Zhang, *Adv. Mater.* **23**, 3061 (2011).
- [31] I. Jung, H. Y. Jang, J. Moon, and S. Park, *Nanoscale* **6**, 6482 (2014).
- [32] J. Bai, X. Zhong, S. Jiang, Y. Huang, and X. Duan, *Nat. Nanotechnol.* **5**, 190 (2010).
- [33] M. Wang, L. Fu, L. Gan, C. Zhang, M. Rummeli, A. Bachmatiuk, K. Huang, Y. Fang, and Z. Liu, *Sci. Rep.* **3**, 1238 (2013).

- [34] B. S. Archanjo, B. Fragneaud, L. Gustavo Cançado, D. Winston, F. Miao, C. Alberto Achete, and G. Medeiros-Ribeiro, *Appl. Phys. Lett.* **104**, 193114 (2014).
- [35] A. Skurativska, S. S. Tsirkin, F. D. Natterer, T. Neupert, and M. H. Fischer, *Phys. Rev. Research* **3**, L032003 (2021).
- [36] J.-Y. You, B. Gu, and G. Su, *Sci. Rep.* **9**, 20116 (2019).
- [37] N. Shima and H. Aoki, *Phys. Rev. Lett.* **71**, 4389 (1993).
- [38] A. Tadjine, G. Allan, and C. Delerue, *Phys. Rev. B* **94**, 075441 (2016).
- [39] R. Saito, A. Jorio, A. G. Souza Filho, G. Dresselhaus, M. S. Dresselhaus, and M. A. Pimenta, *Phys. Rev. Lett.* **88**, 027401 (2001).
- [40] J. Maultzsch, S. Reich, C. Thomsen, H. Requardt, and P. Ordejón, *Phys. Rev. Lett.* **92**, 075501 (2004).
- [41] M. Mohr, J. Maultzsch, E. Dobardžić, S. Reich, I. Milošević, M. Damnjanović, A. Bosak, M. Krisch, and C. Thomsen, *Phys. Rev. B* **76**, 035439 (2007).
- [42] A. Jorio, M. S. Dresselhaus, R. Saito, and G. Dresselhaus, *Raman Spectroscopy in Graphene Related Systems* (Wiley, Weinheim, Germany, 2011).
- [43] A. P. Schnyder, S. Ryu, A. Furusaki, and A. W. W. Ludwig, *Phys. Rev. B* **78**, 195125 (2008).
- [44] S. Ryu, A. P. Schnyder, A. Furusaki, and A. W. W. Ludwig, *New J. Phys.* **12**, 065010 (2010).
- [45] C.-K. Chiu, J. C. Y. Teo, A. P. Schnyder, and S. Ryu, *Rev. Mod. Phys.* **88**, 035005 (2016).
- [46] G. von Gersdorff, S. Panahiyan, and W. Chen, *Phys. Rev. B* **103**, 245146 (2021).
- [47] W. Chen and A. P. Schnyder, *New J. Phys.* **21**, 073003 (2019).
- [48] R. Ortiz, R. A. Boto, N. García-Martínez, J. C. Sancho-García, M. Melle-Franco, and J. Fernández-Rossier, *Nano Lett.* **19**, 5991 (2019).
- [49] L.-K. Lim, J.-N. Fuchs, F. Piéchon, and G. Montambaux, *Phys. Rev. B* **101**, 045131 (2020).
- [50] G. Bouzerar and D. Mayou, *Phys. Rev. B* **103**, 075415 (2021).
- [51] A. H. Castro Neto, F. Guinea, N. M. R. Peres, K. S. Novoselov, and A. K. Geim, *Rev. Mod. Phys.* **81**, 109 (2009).
- [52] F. Liu, F. Qu, I. Žutić, S. Xie, D. Liu, A. L. A. Fonseca, and M. Malard, *J. Phys. Chem. Lett.* **12**, 5710 (2021).
- [53] F. Liu, F. Qu, I. Žutić, and M. Malard, [arXiv:2108.05502](https://arxiv.org/abs/2108.05502).
- [54] M. S. M. de Sousa, F. Liu, M. Malard, F. Qu, and W. Chen, [arXiv:2109.12468](https://arxiv.org/abs/2109.12468).
- [55] S. M. Young and C. L. Kane, *Phys. Rev. Lett.* **115**, 126803 (2015).
- [56] A. Yamakage, Y. Yamakawa, Y. Tanaka, and Y. Okamoto, *J. Phys. Soc. Jpn.* **85**, 013708 (2016).
- [57] Y. X. Zhao and A. P. Schnyder, *Phys. Rev. B* **94**, 195109 (2016).
- [58] B. J. Wieder, B. Bradlyn, Z. Wang, J. Cano, Y. Kim, H.-S. D. Kim, A. M. Rappe, C. L. Kane, and B. A. Bernevig, *Science* **361**, 246 (2018).
- [59] N. B. Kopnin, T. T. Heikkilä, and G. E. Volovik, *Phys. Rev. B* **83**, 220503(R) (2011).
- [60] T. T. Heikkilä and G. Volovik, *Basic Physics of Functionalized Graphite* (Springer, Switzerland, 2016).